Main Manuscript for

Restoring AIBP expression in the retina provides neuroprotection in glaucoma

Authors: Won-Kyu Ju[1]*, Yonju Ha[2], Seunghwan Choi[1], Keun-Young Kim[3], Tonking Bastola[1], Jungsu Kim[4], Robert N. Weinreb[1], Wenbo Zhang[2], Yury I. Miller[4, 5], Soo-Ho Choi[4]*

Affiliations:
[1]Hamilton Glaucoma Center and Shiley Eye Institute, The Viterbi Family Department of Ophthalmology, University of California San Diego, La Jolla, CA 92039, USA.

[2]Department of Ophthalmology and Visual Sciences, University of Texas Medical Branch, TX, 77555-0144, USA.

[3]National Center for Microscopy and Imaging Research, Department of Neurosciences, University of California San Diego, La Jolla, CA 92039, USA.

[4]Department of Medicine, University of California San Diego, La Jolla, CA 92039, USA.

[5]Raft Pharmaceuticals LLC, San Diego, CA 92121, USA

***Correspondence** to Won-Kyu Ju, wju@health.ucsd.edu; Soo-Ho Choi, soc002@health.ucsd.edu

Author Contributions: Conceptualization: W.K.J., Y.I.M., S.H.C.; Methodology: W.K.J., Y.H., K.Y.K., T.B., S.C., J.K., S.H.C.; Investigation: W.K.J., Y.H., K.Y.K., T.B., S.C., J.K., S.H.C.; Visualization: W.K.J., Y.H., K.Y.K., S.H.C.; Funding acquisition: W.K.J., Y.I.M.; Project administration: W.K.J., S.H.C.; Supervision: W.K.J., S.H.C.; Writing – original draft: W.K.J., K.Y.K., Y.I.M., S.H.C.; Writing – review & editing: W.K.J., Y.H., K.Y.K., R.N.W., W.Z., Y.I.M., S.H.C.

Competing Interest Statement: W.K.J., S.H.C. and Y.I.M. are co-inventors named on patents and patent applications by the University of California, San Diego. Y.I.M is a scientific co-founder of Raft Pharmaceuticals LLC. The terms of this arrangement have been reviewed and approved by the University of California, San Diego in accordance with its conflict of interest policies. Other authors declare no competing interests exist.

Classification: Biological Science, Neuroscience.

Keywords: Glaucoma, AIBP, AAV, RGC protection, TLR4-lipid raft.

This PDF file includes:

Main Text
Figures 1 to 5 and Supplementary figures 1 to 4
Supplementary Tables 1 to 4

Abstract

Glaucoma is a neurodegenerative disease manifested in retinal ganglion cell (RGC) death and irreversible blindness. While lowering intraocular pressure (IOP) is the only proven therapeutic strategy in glaucoma, it is insufficient for preventing disease progression, thus justifying the recent focus on targeting retinal neuroinflammation and preserving RGCs. We have identified apolipoprotein A-I binding protein (AIBP) as the protein regulating several mechanisms of retinal neurodegeneration. AIBP controls excessive cholesterol accumulation via upregulating the cholesterol transporter ATP-binding cassette transporter 1 (ABCA1) and reduces inflammatory signaling via toll-like receptor 4 (TLR4) and mitochondrial dysfunction. ABCA1, TLR4 and oxidative phosphorylation components are genetically linked to primary open-angle glaucoma. Here we demonstrated that AIBP and ABCA1 expression was decreased, while TLR4, interleukin 1 β (IL-1β), and the cholesterol content increased in the retina of patients with glaucoma and in mouse models of glaucoma. Restoring AIBP deficiency by a single intravitreal injection of adeno-associated virus (AAV)-AIBP protected RGCs in glaucomatous DBA/2J mice, in mice with microbead-induced chronic IOP elevation, and optic nerve crush. In addition, AIBP expression attenuated TLR4 and IL-1β expression, localization of TLR4 to lipid rafts, reduced cholesterol accumulation, and ameliorated visual dysfunction. These studies collectively indicate that restoring AIBP deficiency in the glaucomatous retina reduces neuroinflammation and protects RGCs and Müller glia, suggesting the therapeutic potential of AAV-AIBP in human glaucoma.

61 **Significance Statement**

62 Lowering intraocular pressure is insufficient to prevent progressive neuroinflammation, retinal
63 ganglion cell (RGC) death and vision loss in glaucoma. We show that reduced expression of
64 AIBP is associated with increased markers of neuroinflammation, TLR4 and IL-1β, in human
65 glaucomatous retina and mouse models of glaucoma. Restoring AIBP expression by an
66 intravitreal injection of AAV-AIBP protects RGCs and preserves visual function in mouse models
67 of glaucoma. Mechanistically, we demonstrate that AAV-AIBP disrupts TLR4-lipid raft formation
68 and attenuates phosphorylation of AMPK, ERK1/2 and p38 and expression of TLR4 and IL-1β *in*
69 *vivo*. Collectively, our findings suggest that AIBP-mediated disruption of retinal TLR4-lipid rafts
70 can prevent RGC loss and demonstrate the therapeutic potential of AAV-AIBP in treatment of
71 human glaucoma.

72
73

Introduction

Glaucoma is a leading cause of blindness worldwide and is characterized by a slow, progressive, and irreversible degeneration of retinal ganglion cells (RGCs) and RGC axons, leading to vision loss (1). Pathophysiological processes leading to the development of glaucoma include elevated intraocular pressure (IOP), glia-driven neuroinflammation, mitochondrial dysfunction, oxidative stress, and vascular dysfunction (2). Currently, elevated IOP is the only proven modifiable risk factor; however, lowering IOP is often not sufficient to prevent glaucoma progression.

Activation of toll-like receptor-4 (TLR4) has been reported as a major component of retinal neuroinflammation. TLR4 polymorphism is associated with the higher risk of glaucoma (3). Elevated IOP increases TLR4 expression, activates inflammasome-associated signaling and induces interleukin-1β (IL-1β)-mediated inflammatory response in retinal degeneration (4, 5). In addition, TLR4 activation is associated with mitochondrial damage caused by intracellular reactive oxygen species (ROS) and defective mitochondrial dynamics (6). This agrees with the report of a polymorphism in mitochondrial cytochrome c oxidase subunit I of the oxidative phosphorylation (OXPHOS) complex (Cx)-IV associated with the development of glaucoma (7). In addition, mitochondrial dysfunction and metabolic stress induced by glaucomatous insults such as elevated IOP result in RGC degeneration (2, 8-10). Genetic deletion or pharmacological inhibition of TLR4 significantly reduces RGC death and proinflammatory responses in experimental glaucoma (11, 12). Our recent study demonstrated that TLR4 and IL-1β expression is upregulated in Müller glia in glaucomatous human and DBA/2J mouse retinas (13). However, clinical development of specific antagonists of TLR4 for multiple indications was so far unsuccessful.

TLR4 activation requires its localization to and homodimerization in lipid rafts, ordered membrane domains with high content of cholesterol and sphingolipids (14-16). Removal of cholesterol from lipid rafts in activated cells disrupts TLR4 signaling (17). Conversely, cholesterol loading of the plasma membrane can activate TLR4-dependent signaling pathways (18). The covariance of membrane cholesterol and TLR4 activation implies that disease-associated dysregulation of cellular cholesterol metabolism and its excessive accumulation may contribute to TLR4 activation. Thus, selective cholesterol depletion from cells expressing high levels of TLR4 would inhibit TLR4 activation and neuroinflammation in glaucoma.

Apolipoprotein A-I binding protein (AIBP; gene name *APOA1BP* or *NAXE*) is a secreted protein that binds apolipoprotein A-I, stabilizes the cholesterol transporter ABCA1 and augments cholesterol efflux (19-21). In addition, AIBP binds to TLR4 and thus directs cholesterol depletion and disruption of lipid rafts to TLR4-expressing cells (14, 22). Recent studies from our group demonstrated that in mouse retina, AIBP was predominantly expressed in RGCs and that AIBP

110 deficiency exacerbated RGC vulnerability to cell death and triggered vision impairment in
111 response to elevated IOP (13). Furthermore, AIBP deficiency was associated with mitochondrial
112 dysfunction in both RGCs and Müller glia and with glia-driven upregulation of the inflammatory
113 TLR4/ IL-1β signaling in glaucomatous neurodegeneration (13).
114 In this study, we found decreased ABCA1 and AIBP expression that was associated with
115 increased TLR4/IL-1β expression and cholesterol deposition in the retina of patients with
116 glaucoma and in mouse models of glaucoma. Using intravitreal delivery of adeno-associated
117 virus (AAV)-AIBP, we demonstrated that restoring AIBP expression inhibited TLR4 activation and
118 IL-1β expression, reduced retinal cholesterol accumulation, protected RGCs and their axon, and
119 ameliorated visual dysfunction in the glaucomatous mouse retina. These results provide *in vivo*
120 evidence that sustained AIBP expression is a key regulator of neuroprotection and may constitute
121 a novel therapeutic strategy for RGC survival and vision preservation in glaucoma.

122 **Results**

123 ***Reduced expression of ABCA1 and AIBP in human glaucomatous retina.***

124 Since ABCA1 has been implicated in glaucoma (25), we conducted an
125 immunohistochemical (IHC) survey of retina specimens from human donors without and with
126 glaucoma diagnosis. The glaucoma diagnosis was confirmed by documenting a significant loss of
127 RGCs and their axons in the optic nerve head (ONH) (*SI Appendix, Fig. S1*). In normal human
128 retina, we observed ABCA1 immunoreactivity in all retinal layers, predominantly localized in RGC
129 somas and axons labeled with neuron-specific β-III tubulin (TUJ1) (Figs. 1 A), and in Müller glia
130 labeled with glutamine synthase (GS) (*SI Appendix,* Fig. S2A). In human glaucomatous retina,
131 the ABCA1 expression was reduced in all retinal layers and significantly diminished in RGCs and
132 Müller glia (Figs. 1 A and C; *SI Appendix,* Fig. S2A). We also found that the patterns of AIBP
133 expression were similar to those for ABCA1 in the control and glaucomatous human retinas and
134 that AIBP was also significantly decreased in the glaucomatous RGCs and Müller glia (Figs. 1 B
135 and C; *SI Appendix,* Fig. S2B).

136 ***Increased cholesterol content and TLR4/IL-1β expression in human glaucomatous retina.***

137 To test whether excessive retinal accumulation of cholesterol occurs in human glaucoma,
138 we performed filipin fluorescent staining. Unesterified cholesterol detected by filipin staining was
139 significantly increased in human glaucomatous compared to normal retina and in the retinal
140 vasculature, suggesting dysregulation of retinal cholesterol metabolism in human glaucoma (Figs.
141 1 D-F). Cholesterol accumulation was associated with increased TLR4 and IL-1β expression in
142 human glaucomatous retina, with a specific pattern of expression in RGC soma and axons, and in

143 Müller glia (Figs. 1 G-H; *SI Appendix, Figs. S2 C and D*). These results suggest that
144 downregulation of ABCA1 and AIBP expression in glaucoma results in increased levels of retinal
145 cholesterol, which in turn leads to plasma membrane reorganization to maintain lipid rafts.
146 Enlarged and stable lipid rafts support increased TLR4 activation and IL-1β expression,
147 contributing to retinal neuroinflammation (Fig. 1J).

148 ***Restoring AIBP expression protects RGCs and their axons in glaucomatous mice.***

149 Based on our findings of reduced AIBP expression in human glaucomatous retina (Figs.
150 1 B and C; *SI Appendix,* Fig. S2B) and in a mouse model of glaucoma (13), we tested the
151 hypothesis that restoring AIBP expression via intravitreal AAV-AIBP delivery would reduce RGC
152 death in glaucomatous DBA/2J (further referred to as D2) mice. We intravitreally injected AAV-
153 Null or AAV-AIBP at the age of 5 months and then assessed RGC survival and axon preservation
154 at the age of 10 months (Fig. 2A). We used D2-*Gpnmb*$^{+}$ mice, which do not develop a glaucoma-
155 like pathology, injected with AAV-Null, as an age-matched control. To reduce the effect of IOP
156 variation in this model, we further selected mice that have had IOP in the range of 20-35 mmHg
157 (Fig. 2B; *SI Appendix, Table S1*) (8). We found that AIBP expression was restored in AIBP-D2
158 mice but not Null-D2 mice (Figs. 2 C and D).

159 In comparison with non-glaucomatous Null-D2-*Gpnmb*$^{+}$ mice, elevated IOP resulted in a
160 significant loss of RGCs in glaucomatous Null-D2 mice (Figs. 2 E and F; *SI Appendix, Table S1*).
161 Remarkably, administration of AAV-AIBP significantly reduced RGC death in D2 mice compared
162 with Null-D2 mice (Figs. 2 E and F; *SI Appendix, Table S1*). We further found that administration
163 of AAV-AIBP significantly increased microglial branch length and number of endpoints in the
164 middle area of the retina, without changes in the soma size or the number of IBA1-positive
165 microglia (Figs. 2 G and H), suggesting that AIBP protects RGCs by preventing microglia
166 activation in glaucomatous neurodegeneration. Furthermore, administration of AAV-AIBP also
167 preserved RGC axons in the ONH (glial laminar area) in D2 mice (Fig. 2I).

168 We next examined effect of restoring AIBP expression on RGC protection in a mouse
169 model of microbead (MB)-induced ocular hypertension (26, 27). We intravitreally injected six-
170 week-old C57BL/6J mice with AAV-Null or AAV-AIBP at 3 weeks before the MB injection. We
171 then measured IOP weekly and counted RGC numbers at 8 weeks after MB injection (Figs. 2 J
172 and K; *SI Appendix, Table S2*). In comparison with non-glaucomatous AAV-Null-control (Null-
173 CNT) mice, MB-induced IOP elevation in AAV-Null mice (Null-MB) resulted in a significant loss of
174 RGCs (Figs. 2 L and M; *SI Appendix, Table S2*). Importantly, administration of AAV-AIBP
175 significantly reduced RGC death in MB mice (Figs. 2 L and M; *SI Appendix, Table S2*).

176 ***Restoring AIBP expression ameliorates visual dysfunction in glaucomatous axon injury.***

177 Optic nerve crush (ONC) is often used as a model of traumatic optic neuropathy or
178 glaucomatous axon injury because it shows similar pathological phenotypes of RGC soma and
179 axon degeneration following the injury. To examine the effect of restoring AIBP expression on
180 RGC protection in ONC injury, we intravitreally injected AAV-Null or AAV-AIBP into the eyes of 4-
181 month-old C57BL/6J mice at 3 weeks before ONC and then counted RGC numbers at 1 week
182 after ONC (Fig. 3A). Consistent with other experimental models of glaucoma, administration of
183 AAV-AIBP significantly reduced RGC death in ONC mice (Figs. 3 B and C; *SI Appendix, Table*
184 *S3*). To determine the effect of restoring AIBP expression on visual function, we next measured
185 1) RGC function using the pattern electroretinogram (PERG), a measurement of the electrical
186 activity by RGCs during exposure to a visual stimulus and 2) the maximum spatial frequency that
187 could elicit head tracking ("acuity") in a virtual-reality optomotor system. In comparison with AAV-
188 Null-CNT mice, ONC resulted in a significant loss of PERG amplitudes in Null-ONC mice (Figs. 3
189 D and E). Importantly, administration of AAV-AIBP significantly recovered PERG amplitudes in
190 AIBP-ONC mice (Figs. 3 D and E). In addition, ONC resulted in a significant reduction of visual
191 acuity by decreasing spatial frequency in Null-ONC (Fig. 3 F). However, administration of AAV-
192 AIBP significantly restored visual acuity by increasing spatial frequency in AIBP-ONC mice (Fig. 3
193 F).

194 ***AIBP reduces cholesterol deposition and inhibits TLR4/IL-1β expression in the retina of***
195 ***glaucomatous D2 mice.***

196 We found decreased TUJ1 immunoreactivity in RGC neurites in the inner plexiform layer
197 and in the RGC somas and axons of the GCL of Null-D2 mice that was significantly increased by
198 administration of AAV-AIBP (Figs. 4 A and B). Since AIBP can facilitate removal of excessive
199 cholesterol from activated cells (20, 28, 29) and because we found an increased cholesterol
200 deposition in the retina of unchallenged AIBP-deficient mice (*SI Appendix,* Fig. S3), we next
201 examined whether administration of AAV-AIBP reduces excessive cholesterol accumulation in the
202 glaucomatous D2 retina. We observed a significant increase of cholesterol deposition in all retinal
203 layers of glaucomatous Null-D2 mice compared with Null-D2-*Gpnmb*$^{+}$ mice, which was
204 significantly decreased in AIBP-D2 mice (Figs. 4 C and D), suggesting that restoring retinal AIBP
205 expression can reduce cholesterol deposition and protect RGC somas and dendrites, even under
206 conditions of elevated IOP.

207 Because glaucomatous D2 retina shows significant increase in TLR4 expression (13) and
208 AIBP plays a role in disrupting TLR4 signaling via removal of excessive cholesterol from activated
209 cells in neuropathic pain states (14, 22), we further examined whether restoring AIBP expression

210 inhibits activation of TLR4 in glaucomatous D2 retina. We observed a significant increase of
211 TLR4 expression, TLR4-associated lipid rafts as measured by a proximity ligation assay, and IL-
212 1β expression in glaucomatous Null-D2 retina compared with Null-D2-*Gpnmb*$^+$ retina, which were
213 all significantly reduced in AIBP-D2 retina (Figs. 4 E-I). These findings suggest that restoring
214 retinal AIBP expression reduces cholesterol deposition and TLR4-lipid raft formation and inhibits
215 TLR4/IL-1β expression, leading to inhibition of neuroinflammation and RGC protection in
216 experimental mouse models of glaucoma (Fig. 4J).

217 ***AIBP expression reduces MAPK and AMPK activation in the retina of glaucomatous D2***
218 ***mice.***

219 Because MAP kinase-mediated signaling pathways are associated with the activation of
220 retinal glial cells (astrocytes or Müller glia) in the glaucomatous human retina (30), we first
221 examined the expression levels and distribution of phospho-p38 (pp38) and phospho-ERK1/2
222 (pEKR1/2) in the glaucomatous human retina. In the control human retina, we observed that pp38
223 immunoreactivity was present in Müller glia and neuronal cells in the inner nuclear layer (INL) (*SI*
224 *Appendix,* Fig. S4A and B). In the glaucomatous human retina, we found an increase of pp38
225 immunoreactivity in RGCs and Müller glia (*SI Appendix,* Fig. S4A-C). Consistently, we found a
226 significantly increased pp38 in Null-D2 retina compared with Null-D2-*Gpnmb*$^+$ retina in RGCs (*SI*
227 *Appendix,* Fig. S4D-F). Administration of AAV-AIBP significantly reduced pp38 in the inner retinal
228 layer and TUJ1-positive RGCs in AIBP-D2 retina (*SI Appendix,* Fig. S4D-F). In addition, in the
229 control human retina, we observed that pERK1/2 immunoreactivity was present in Müller glia (*SI*
230 *Appendix,* Fig. S4H), and that it was increased in Müller glia in the inner retinal layers of the
231 glaucomatous human retina (*SI Appendix,* Fig. S4H and I). Interestingly, we did not detect
232 pERK1/2 immunoreactivity in RGCs from both normal and glaucomatous human retinas (*SI*
233 *Appendix,* Fig. S4G). Consistent with human data, we found significantly increased pERK1/2 in
234 Null-D2 retina compared with Null-D2-*Gpnmb*$^+$ retina (*SI Appendix,* Fig. S4J), which was reduced
235 to normal levels in AIBP-D2 retina (*SI Appendix,* Fig. S4J). As in human retina, pERK1/2 was
236 detected in other than TUJ1-positive cells (*SI Appendix,* Fig. S4J). These results were replicated
237 in pERK1/2 IHC analyses (*SI Appendix,* Fig. S4K and L).

238 AMPK is a highly conserved energy sensor and its hyperactivation is prominent in RGCs
239 from experimental glaucoma and patients with primary open-angle glaucoma (POAG) (31).
240 Attenuation of AMPK hyperactivation promotes RGC function and survival by inhibiting dendritic
241 retraction and synaptic loss in magnetic microbead occlusion mouse model of glaucoma (32). We
242 observed that pAMPK (Thr172) immunoreactivity in Müller glia and RGCs was significantly
243 increased in human glaucomatous compared to normal retina (Figs. 5 A-C). Consistent with the

244 human data, we found significantly increased pAMPK in Null-D2 retina compared with Null-D2-
245 *Gpnmb*$^{+}$ retina (Fig. 5D). Restoring AIBP expression significantly decreased pAMPK in
246 glaucomatous AIBP-D2 retina as measured by western blot (Fig. 5D). IHC analysis also showed
247 increased pAMPK in Null-D2 RGCs compared with Null-D2-*Gpnmb*$^{+}$ RGCs (Figs. 5 E and F) and
248 that restoring AIBP expression decreased pAMPK in both OPL and inner retinal layers of AIBP-
249 D2 mice (Figs. 5 E and F). These results support the notion that retinal AIBP expression delivered
250 by an AAV protects RGCs and improves axonal transport via inhibition of inflammation and
251 restoration of energy homeostasis (Fig. 5G).

252 **Discussion**

253 In this study, we report novel findings of significantly reduced ABCA1 and AIBP
254 expression as well as increased cholesterol accumulation that are associated with increasing of
255 TLR4 and IL-1β expression in the retina of human patients with glaucoma. These findings were
256 replicated in a mouse experimental model of glaucoma. The excessive retinal cholesterol
257 deposition was reversed by restoring AIBP expression via a single intravitreal injection of AAV-
258 AIBP. This treatment reduced TLR4 and IL-1β expression and it prevented RGC loss and visual
259 dysfunction in mouse models of glaucoma. The neuroprotective AIBP effect was mediated by
260 reducing phosphorylation of AMPK, p38, and ERK1/2, as well as reducing inflammatory response
261 by glaucomatous insults such as elevated pressure.

262 We identified AIBP as a master regulator of retinal cholesterol content, which in turn
263 regulates retinal neuroinflammation and RGC survival. The causes of reduced AIBP expression in
264 glaucoma are yet to be elucidated, but an AAV-AIBP intervention to restore AIBP expression
265 normalized retinal cholesterol, disrupted TLR4-lipid raft formation, inhibited TLR4 and IL-1β
266 expression and prevented RGS loss. AIBP is a 32 kDa protein, which depending on
267 phosphorylation by PKA, can be secreted or localized to mitochondria (19, 33). The AAV-AIBP
268 construct employed in our studies contains a strong secretion signal (fibronectin signal peptide),
269 thus the observed effects can be assigned to a secreted form of AIBP. We and others have
270 reported that the secreted, extracellular AIBP facilitates removal of excess cholesterol from
271 endothelial cells and macrophages, resulting in reduction of lipid rafts and inhibition of
272 angiogenesis, atherosclerosis and pulmonary inflammation (20, 21, 28, 29, 34). More recently, we
273 have shown that AIBP binds to TLR4 and mediates selective cholesterol depletion and disruption
274 of lipid rafts in TLR4-expressing cells. The loss of lipid raft integrity in microglia results in inhibition
275 of TLR4 dimerization and reduced spinal neuroinflammation (22, 35). Moreover, AIBP
276 downregulates the surface expression and function of TLR4 and downstream inflammatory
277 pathways in macrophages and microglia (14, 36, 37). In this study, we observed AIBP-mediated
278 reductions in retinal TLR4 expression and TLR4 localization to lipid rafts.

279 It is established that TLR4 activation simultaneously triggers the activation of MAPK/NF-

280 κB and inflammasome pathways, thereby escalating the secretion of proinflammatory cytokines
281 (4, 5, 38). In the current study, we found that phosphorylation of p38 was increased in both RGCs
282 and Müller glia in the glaucomatous human retina, while phosphorylation of ERK1/2 was
283 increased only in Müller glia. The MAPK signaling has been known to regulate not only
284 inflammatory response (39) but also mitochondrial biogenesis (40, 41). Here, we found that AIBP
285 administration significantly reduced phosphorylation of p38 and ERK1/2 in the inner retinal layer
286 of the glaucomatous D2 mice. Together, these findings suggest that the AIBP administration
287 leading to normalization of TLR4-associated lipid rafts may preserve mitochondrial function and
288 inhibit inflammatory responses by preventing activation of the MAPK pathways under
289 glaucomatous injury and thus protecting RGCs.
290 Human glaucomatous retina and the retinas in mouse models of glaucoma are
291 characterized by biomarkers of energy depletion and metabolic vulnerability (32, 42, 43), which
292 are associated with inflammatory response (43). AMPK is a highly conserved metabolic energy
293 sensor activated by a variety of energy stresses and mitochondrial damage that reduce ATP
294 levels (44, 45). Because mitochondrial dysfunction produces a low level of ATP and leads to
295 axonal and dendritic degeneration in RGCs (13, 32), AMPK activation would be a
296 pathophysiological indicator for glaucomatous RGC degeneration. Indeed, AMPK activation has
297 been found in experimental mouse models of glaucoma (32, 43). Here, we showed that AIBP
298 administration significantly inhibited AMPK activation in RGCs and Müller glia in the
299 glaucomatous mouse retina, implying that AIBP may protect RGCs and Müller glia by
300 ameliorating energy crisis and metabolic stress induced by glaucomatous insults.
301 In conclusion, we propose the novel paradigm that controlling TLR4-lipid rafts in the
302 retina – via maintenance of retinal expression of secreted AIBP – can protect RGCs under the
303 conditions of elevated IOP. The mechanism includes inhibition of TLR4-lipid raft activation, and
304 reduced activation of glaucomatous Müller glia, leading to RGC protection and preservation of
305 visual function *(SI Appendix, Figs. S5*).

306

307 **Materials and Methods**

308 ***Human tissue samples.*** Human retina tissue sections were obtained, via San Diego Eye Bank,
309 from two eyes of a donor (age 85 years) without history of glaucoma or any other eye disease,
310 and of glaucoma patients (ages 76 and 84 years). The studies were approved by the University of
311 California, San Diego Human Research Protection Program. Both control and glaucoma patients
312 had no history of other eye disease, diabetes, or chronic central nervous system disease.

313 ***Animals.*** Adult male and female DBA/2J and age-matched D2-*Gpnmb*$^{+}$ mice (The Jackson
314 Laboratory), and WT and *Apoa1bp*$^{-/-}$ mice were housed in covered cages, fed with a standard
315 rodent diet ad libitum, and kept on a 12 h light/12 h dark cycle. C57BL/6J mice were initially
316 purchased from the Jackson Laboratory, bred in-house for experiments and used as WT mice.
317 *Apoa1bp*$^{-/-}$ mice on a C57BL/6J background were generated in our group as previously reported
318 (28, 34). Animals were assigned randomly to experimental and control groups. All procedures
319 concerning animals were in accordance with the Association for Research in Vision and
320 Ophthalmology Statement for the Use of Animals in Ophthalmic Vision Research and under
321 protocols approved by Institutional Animal Care and Use Committee at the University of
322 California, San Diego and the University of Texas Medical Branch.

323 ***Production of recombinant AAV-AIBP vector.*** AAV-AIBP was generated as previously
324 reported (46). Murine AIBP (25-283aa) was fused with FIB at the N-terminus and 6x-His at the C-
325 terminus (FIB-AIBP-His). FIB-AIBP-His was transduced by the AAV-DJ/8 Helper-free system
326 (Cell BioLabs) which is mimicking serotypes AAV8 and AAV9 with the inverted terminal repeats
327 (ITRs) from AAV2 (Agilent Technologies) that contains the CMV promoter and subsequently
328 purified according to published protocol (47). AAV was titrated using quantitative PCR (qPCR)
329 with primers for the ITR sequence (TaKaRa Bio Inc).

330 ***Transduction with recombinant AAV constructs.*** The 5-month-old pre-glaucomatous DBA/2J
331 and D2-*Gpnmb*$^{+}$ mice were anesthetized with an intraperitoneal (IP) injection of a mixture of
332 ketamine/xylazine and topical 1% proparacaine eye drops. A 32-gauge needle was used to inject
333 a total of 1 µl of either AAV-Null or AAV-AIBP ($1x10^{13}$ gc/ml) into the vitreous humor of the eye.
334 Injections were given slowly over 1 min and the needle was maintained in position for an
335 additional 10 min to minimize vector loss through the injection tract. At the age of 10 months, the
336 mice were euthanized by an IP injection of a mixture of ketamine/xylazine, and the retina and
337 ONH tissues were prepared.

338 ***Mouse model of MB-induced ocular hypertension.*** MB-induced glaucoma was induced using
339 a modified protocol based on previous publications (26, 27). In brief, six-week-old C57BL/6J mice

340 were intravitreally injected with either AAV-Null or AAV-AIBP as described above. At 3 weeks
341 post-injection, mice were anesthetized by an IP injection of a cocktail of ketamine (100 mg/kg,
342 Ketaset; Fort Dodge Animal Health) and xylazine (9 mg/kg, TranquiVed; VEDCO Inc.). We
343 topically applied 0.5% proparacaine hydrochloride and the pupils were dilated with 1%
344 tropicamide and 2.5% phenylephrine and then the cornea was gently punctured using a 30-gauge
345 needle. Next, 2 µl of 1-µm-diameter polystyrene MB suspension (containing 3.0×10^7 beads)
346 followed by an air bubble, 2 µl of 6-µm-diameter polystyrene MB suspension (containing $6.3 \times$
347 10^6 beads, Polysciences), and 1 µl of PBS containing 30% Healon was injected into the anterior
348 chamber using a 32-gauge needle (Hamilton Company) connected to a syringe (Hamilton
349 Company), which induced moderate elevation of IOP for ≥6 wk. An equivalent volume of PBS
350 was injected into the contralateral eyes to serve as sham control. At 8 weeks after the MB
351 injection, mice were sacrificed, and the retina tissues were prepared.

352 ***IOP measurement.*** IOP elevation onset in DBA/2J mice typically occurs between 5 and 7 months
353 of age, and by 9 to 10 months of age, IOP-linked optic nerve axon loss is well advanced (8, 9).
354 IOP measurements were performed as previously described (8, 9). Each of the 10-month-old D2-
355 *Gpnmb*$^+$ and DBA/2J mice used in this study had a single IOP measurement (to confirm
356 development of spontaneous IOP elevation exceeding 20 mmHg) using a tonometer (TonoLab,
357 Colonial Medical Supply) (n = 24 mice per group). For the mouse model of MB-induced
358 glaucoma, IOP was measured using a tonometer (TonoLab) from 3 days after MB injection
359 thereafter until 6 weeks after injection between 3 p.m. and 5 p.m. to minimize diurnal variability.
360 Non-IOP elevation contralateral control retinas were used as sham control (n = 9-11 mice per
361 group).

362 ***Tissue preparation.*** Mice were anesthetized by an IP injection of a cocktail of ketamine/xylazine
363 as described above prior to cervical dislocation. For immunohistochemistry, the retinas and ONHs
364 were dissected from the eyeballs and fixed with 4% paraformaldehyde (Sigma) in PBS (pH 7.4)
365 for 2 h at 4 °C. Retinas were washed several times with PBS then dehydrated through graded
366 levels of ethanol and embedded in polyester wax. For EM, the eyes were fixed via cardiac
367 perfusion with 2% paraformaldehyde, 2.5% glutaraldehyde (Ted Pella) in 0.15 M sodium
368 cacodylate (pH 7.4, Sigma) solution at 37 °C and placed in pre-cooled fixative of the same
369 composition on ice for 1 h. As described below, the procedure was used to optimize mitochondria
370 structural preservation and membrane contrast. For western blot analyses, extracted retinas were
371 immediately used.

372 ***Western blot analyses.*** Harvested retinas were homogenized for 1 min on ice with a RIPA lysis
373 buffer (Cell Signaling Technology), containing protease inhibitor cocktail (MedChemExpress). The

374 lysates were then centrifuged at 13,000 rpm for 15 min and protein amounts in the supernatants
375 were measured by DC Protein assay (Bio-Rad). Proteins (10-20 μg) were run on a NuPAGE Bis-
376 Tris gel (Invitrogen) and transferred to polyvinylidene difluoride membranes (PVDF) membranes
377 (GE Healthcare Bio-Science). The membranes were blocked with TBS/0.1% Tween-20 (T-TBS)
378 containing 5% bovine serum albumin (BSA) for 1 h at room temperature and incubated with
379 primary antibodies for overnight at 4 °C. Membrane were washed three times with T-TBS then
380 incubated with horseradish peroxidase (HRP)-conjugated secondary antibodies (Cell Signaling
381 Technology) for 1 h at room temperature. Membranes were developed using enhanced
382 chemiluminescence substrate system (ThermoFisher Scientific). The images were captured using
383 a UVP imaging system.

384 ***Immunohistochemistry*.** Immunohistochemical staining of 7 μm wax sections of full thickness
385 retina were performed. Sections from wax blocks from each group were used for
386 immunohistochemical analysis. To prevent non-specific background, tissues were incubated in
387 1% BSA/PBS for 1 h at room temperature before incubation with the primary antibodies for 16 h
388 at 4°C. After several wash steps, the tissues were incubated with the secondary antibodies for 4
389 h at 4°C and subsequently washed with PBS. The sections were counterstained with the nucleic
390 acid stain Hoechst 33342 (1 μg/ml; Invitrogen) in PBS. Images were acquired with Keyence All-
391 in-One Fluorescence microscopy (BZ-X810, Keyence Corp. of America). Each target protein
392 fluorescent integrated intensity in pixel per area was measured using the ImageJ software
393 (National Institutes of Health). All imaging parameters remained the same and were corrected
394 with the background subtraction.

395 ***Whole-mount immunohistochemistry and RGC counting*.** Mouse retinas from enucleated
396 eyes were dissected as flattened whole-mounts. Retinas were immersed in PBS containing 30%
397 sucrose for 24 h at 4°C. The retinas were blocked in PBS containing 3% donkey serum, 1% BSA,
398 1% fish gelatin and 0.1% triton X-100, and incubated with primary antibodies for 3 days at 4°C.
399 Primary antibodies used were rabbit polyclonal anti-RBPMS antibody or mouse monoclonal anti-
400 TUJ1 antibody. After several wash steps, the retinas were incubated with Alexa Fluor-488
401 conjugated donkey anti-rabbit IgG antibody or Alexa Fluor-568 conjugated donkey anti-mouse
402 IgG antibody for 24 h, and subsequently washed with PBS. Images were acquired with Keyence
403 All-in-One Fluorescence microscopy (BZ-X810, Keyence Corp. of America). RBPMS- or TUJ1-
404 positive RGCs were counted in four regions within the middle and/or peripheral retina (three
405 sixths for middle and five sixths for peripheral of the retinal radius) and the scores were averaged
406 using ImageJ.

407 ***Microglia morphology analysis*.** Whole-mounted mouse retinas were stained with IBA-1
408 antibody and z-stack images were acquired with Olympus FluoView 1000 confocal microscope
409 (Olympus) with 20x magnification. For microglia morphology analysis, branch length, number of
410 endpoints, soma size, and number of microglia were measured using ImageJ as described (48).

411 ***Filipin staining*.** Fluorescence probe filipin binds to unesterified cholesterol in biological
412 membranes. Frozen retina sections were immersed in PBS for 10 min. The sections were
413 incubated with 1.5 mg/ml glycine (Sigma-Aldrich) for 10 min and followed by staining with 50
414 µg/ml filipin (Sigma-Aldrich) for 2 h at room temperature in the dark. The sections were washed 3
415 times with PBS and counter stained with DRAQ5 (BioLegend) to stain DNA for 10 min. Images
416 were acquired with an Olympus FluoView1000 confocal microscopy (Olympus). The fluorescent
417 integrated intensity in pixel per area was measured using the ImageJ. All imaging parameters
418 remained the same and were corrected with the background subtraction.

419 ***PERG analysis.*** PERG recordings were performed by Celeris ERG platform equipped with
420 pattern ERG stimulators (Diagnosys LLC) (49). Following anesthesia and eye dilation pattern,
421 ERG stimulators were placed on corneal surface. PERG amplitude was measured between first
422 positive peak (P1) and second negative peak (N2).

423 ***Virtual optomotor response analysis.*** Spatial visual function was performed on a virtual
424 optomotor system (OptoMotry; CerebralMechanics Inc., AB, Canada) (13). Spatial frequency
425 threshold, a measure of visual acuity, was determined automatically with accompanying
426 OptoMotry software, which uses a step-wise paradigm based upon head-tracking movements at
427 100% contrast.

428 ***Proximity ligation assay (PLA)*.** The PLA oligo/probe-conjugated mouse anti-TLR4 (BioLegend)
429 and goat anti-cholera toxin subunit B (CTB, Sigma) antibodies were created using Duolink® PLA
430 probemaker (Sigma-Aldrich) according to the manufacturer's instructions. To measure TLR4-
431 associated lipid raft (GM1 ganglioside) formation, Duolink® Proximity ligation assay (PLA, Sigma)
432 was performed by following the manufacturer's instructions. Briefly, frozen retina sections were
433 immersed in H_2O for 5 min at room temperature. The sections were blocked with one drop of
434 Duolink blocking buffer for 1 h at 37°C. For lipid raft staining, the sections were first incubated
435 with 5 µg/ml of unconjugated CTB (Sigma) for 45 min at 37°C. The oligo/probe-conjugated anti-
436 mouse TLR4 and anti-goat CTB antibodies (1:100) were added to the sections and incubated for
437 additional 2 h at 37°C. The sections were washed twice with Duolink wash buffer, incubated with
438 ligation mixture for 30 min 37°C, followed by incubating with amplification mixture overnight at

439 37°C. Next day, the sections were washed and incubated with detection buffer for 30 min at
440 37°C. Images were acquired with Keyence All-in-One Fluorescence microscopy. Each TLR4-CTB
441 PLA fluorescent integrated intensity in pixel per area was measured using the ImageJ. All
442 imaging parameters remained the same and were corrected with the background subtraction.

443 ***Statistical analyses.*** All results were reported as means ± SEM. For comparison between two
444 groups, statistical analysis was performed using a two-tailed Student's t-test. For multiple group
445 comparisons, we used one-way analysis of variance (ANOVA) and Tukey's multiple comparisons
446 test, using GraphPad Prism. A P value less than 0.05 was considered statistically significant. *P <
447 0.05, **P < 0.01, ***P < 0.001, ****P < 0.0001. The value of n per group is indicated within each
448 figure legend.

449 **Acknowledgments**

450 The authors thank Dr. Shenglin Li for creating illustrative diagrams. This work was supported by
451 the National Institutes of Health grants EY031697 (W.K.J.), AG081004 (W.K.J.), EY034116
452 (W.K.J./K.Y.K/S.H.C), NS129684 (W.K.J.), EY034376 (W.Z.), EY022694 (W.Z.), EY026629
453 (W.Z.), HL136275 (Y.I.M.), AG081037 (Y.I.M./W.K.J.), and P30 EY022589 (Core Vision
454 Research).
455

456 **References**

457 1. R. N. Weinreb *et al.*, Primary open-angle glaucoma. *Nat Rev Dis Primers* **2**, 16067
458 (2016).
459 2. G. Tezel, Multifactorial Pathogenic Processes of Retinal Ganglion Cell Degeneration in
460 Glaucoma towards Multi-Target Strategies for Broader Treatment Effects. *Cells* **10**
461 (2021).
462 3. J. Navarro-Partida *et al.*, Association of Toll-like receptor 4 single-nucleotide
463 polymorphisms Asp299Gly and Thr399Ile with the risk of primary open angle glaucoma.
464 *Graefes Arch Clin Exp Ophthalmol* **255**, 995-1001 (2017).
465 4. Y. Qi *et al.*, Retinal ischemia/reperfusion injury is mediated by Toll-like receptor 4
466 activation of NLRP3 inflammasomes. *Invest Ophthalmol Vis Sci* **55**, 5466-5475 (2014).
467 5. W. Chi *et al.*, Caspase-8 promotes NLRP1/NLRP3 inflammasome activation and IL-1beta
468 production in acute glaucoma. *Proc Natl Acad Sci U S A* **111**, 11181-11186 (2014).
469 6. S. Y. Kim *et al.*, Isorhamnetin alleviates lipopolysaccharide-induced inflammatory
470 responses in BV2 microglia by inactivating NF-kappaB, blocking the TLR4 pathway and
471 reducing ROS generation. *Int J Mol Med* **43**, 682-692 (2019).
472 7. D. W. Collins *et al.*, The MT-CO1 V83I Polymorphism is a Risk Factor for Primary Open-
473 Angle Glaucoma in African American Men. *Invest Ophthalmol Vis Sci* **59**, 1751-1759
474 (2018).
475 8. W. K. Ju *et al.*, Intraocular pressure elevation induces mitochondrial fission and triggers
476 OPA1 release in glaucomatous optic nerve. *Invest Ophthalmol Vis Sci* **49**, 4903-4911
477 (2008).
478 9. K. Y. Kim *et al.*, DRP1 inhibition rescues retinal ganglion cells and their axons by
479 preserving mitochondrial integrity in a mouse model of glaucoma. *Cell Death Dis* **6**,
480 e1839 (2015).

481 10. M. Harun-Or-Rashid *et al.*, Structural and Functional Rescue of Chronic Metabolically
482 Stressed Optic Nerves through Respiration. *J Neurosci* **38**, 5122-5139 (2018).
483 11. Y. Nakano *et al.*, Toll-like receptor 4 inhibitor protects against retinal ganglion cell
484 damage induced by optic nerve crush in mice. *J Pharmacol Sci* **133**, 176-183 (2017).
485 12. D. Morzaev *et al.*, Toll-like receptor-4 knockout mice are more resistant to optic nerve
486 crush damage than wild-type mice. *Clin Exp Ophthalmol* **43**, 655-665 (2015).
487 13. S. H. Choi *et al.*, AIBP protects retinal ganglion cells against neuroinflammation and
488 mitochondrial dysfunction in glaucomatous neurodegeneration. *Redox Biol* **37**, 101703
489 (2020).
490 14. S. A. Woller *et al.*, Inhibition of Neuroinflammation by AIBP: Spinal Effects upon
491 Facilitated Pain States. *Cell Rep* **23**, 2667-2677 (2018).
492 15. A. R. Tall, L. Yvan-Charvet, Cholesterol, inflammation and innate immunity. *Nat Rev*
493 *Immunol* **15**, 104-116 (2015).
494 16. X. Zhu *et al.*, Macrophage ABCA1 reduces MyD88-dependent Toll-like receptor
495 trafficking to lipid rafts by reduction of lipid raft cholesterol. *J Lipid Res* **51**, 3196-3206
496 (2010).
497 17. M. B. Fessler, J. S. Parks, Intracellular lipid flux and membrane microdomains as
498 organizing principles in inflammatory cell signaling. *J Immunol* **187**, 1529-1535 (2011).
499 18. Y. Sun *et al.*, Free cholesterol accumulation in macrophage membranes activates Toll-
500 like receptors and p38 mitogen-activated protein kinase and induces cathepsin K. *Circ*
501 *Res* **104**, 455-465 (2009).
502 19. M. Ritter *et al.*, Cloning and characterization of a novel apolipoprotein A-I binding protein,
503 AI-BP, secreted by cells of the kidney proximal tubules in response to HDL or ApoA-I.
504 *Genomics* **79**, 693-702 (2002).
505 20. L. Fang *et al.*, Control of angiogenesis by AIBP-mediated cholesterol efflux. *Nature* **498**,
506 118-122 (2013).
507 21. M. Zhang *et al.*, Apolipoprotein A-1 binding protein promotes macrophage cholesterol
508 efflux by facilitating apolipoprotein A-1 binding to ABCA1 and preventing ABCA1
509 degradation. *Atherosclerosis* **248**, 149-159 (2016).
510 22. J. M. Navia-Pelaez *et al.*, Normalization of cholesterol metabolism in spinal microglia
511 alleviates neuropathic pain. *J Exp Med* **218** (2021).
512 23. L. Jacobo-Albavera, M. Dominguez-Perez, D. J. Medina-Leyte, A. Gonzalez-Garrido, T.
513 Villarreal-Molina, The Role of the ATP-Binding Cassette A1 (ABCA1) in Human Disease.
514 *Int J Mol Sci* **22** (2021).
515 24. X. Zhu *et al.*, Increased cellular free cholesterol in macrophage-specific Abca1 knock-out
516 mice enhances pro-inflammatory response of macrophages. *J Biol Chem* **283**, 22930-
517 22941 (2008).
518 25. P. Gharahkhani *et al.*, Common variants near ABCA1, AFAP1 and GMDS confer risk of
519 primary open-angle glaucoma. *Nat Genet* **46**, 1120-1125 (2014).
520 26. W. Liu *et al.*, Neuronal Epac1 mediates retinal neurodegeneration in mouse models of
521 ocular hypertension. *J Exp Med* **217** (2020).
522 27. R. M. Sappington, B. J. Carlson, S. D. Crish, D. J. Calkins, The microbead occlusion
523 model: a paradigm for induced ocular hypertension in rats and mice. *Invest Ophthalmol*
524 *Vis Sci* **51**, 207-216 (2010).
525 28. D. A. Schneider *et al.*, AIBP protects against metabolic abnormalities and
526 atherosclerosis. *J Lipid Res* **59**, 854-863 (2018).
527 29. S. H. Choi *et al.*, AIBP augments cholesterol efflux from alveolar macrophages to
528 surfactant and reduces acute lung inflammation. *JCI Insight* **3** (2018).
529 30. G. Tezel, B. C. Chauhan, R. P. LeBlanc, M. B. Wax, Immunohistochemical assessment
530 of the glial mitogen-activated protein kinase activation in glaucoma. *Invest Ophthalmol*
531 *Vis Sci* **44**, 3025-3033 (2003).
532 31. K. Burkewitz, Y. Zhang, W. B. Mair, AMPK at the nexus of energetics and aging. *Cell*
533 *Metab* **20**, 10-25 (2014).

534 32. N. Belforte *et al.*, AMPK hyperactivation promotes dendrite retraction, synaptic loss, and
535 neuronal dysfunction in glaucoma. *Mol Neurodegener* **16**, 43 (2021).
536 33. A. Y. Marbaix *et al.*, Occurrence and subcellular distribution of the NADPHX repair
537 system in mammals. *Biochem J* **460**, 49-58 (2014).
538 34. R. Mao *et al.*, AIBP Limits Angiogenesis Through gamma-Secretase-Mediated
539 Upregulation of Notch Signaling. *Circ Res* **120**, 1727-1739 (2017).
540 35. Y. Liu, C. Tang, Regulation of ABCA1 functions by signaling pathways. *Biochim Biophys*
541 *Acta* **1821**, 522-529 (2012).
542 36. M. Zhang *et al.*, AIBP reduces atherosclerosis by promoting reverse cholesterol transport
543 and ameliorating inflammation in apoE(-/-) mice. *Atherosclerosis* **273**, 122-130 (2018).
544 37. L. Fang, Y. I. Miller, Regulation of lipid rafts, angiogenesis and inflammation by AIBP.
545 *Curr Opin Lipidol* **30**, 218-223 (2019).
546 38. T. Duan, Y. Du, C. Xing, H. Y. Wang, R. F. Wang, Toll-Like Receptor Signaling and Its
547 Role in Cell-Mediated Immunity. *Front Immunol* **13**, 812774 (2022).
548 39. Y. J. Kang *et al.*, Macrophage deletion of p38alpha partially impairs lipopolysaccharide-
549 induced cellular activation. *J Immunol* **180**, 5075-5082 (2008).
550 40. D. Knutti, D. Kressler, A. Kralli, Regulation of the transcriptional coactivator PGC-1 via
551 MAPK-sensitive interaction with a repressor. *Proc Natl Acad Sci U S A* **98**, 9713-9718
552 (2001).
553 41. J. Prieto *et al.*, Early ERK1/2 activation promotes DRP1-dependent mitochondrial fission
554 necessary for cell reprogramming. *Nat Commun* **7**, 11124 (2016).
555 42. S. Lee *et al.*, Mitochondrial dysfunction in glaucoma and emerging bioenergetic
556 therapies. *Exp Eye Res* **93**, 204-212 (2011).
557 43. M. Harun-Or-Rashid, D. M. Inman, Reduced AMPK activation and increased HCAR
558 activation drive anti-inflammatory response and neuroprotection in glaucoma. *J*
559 *Neuroinflammation* **15**, 313 (2018).
560 44. F. Moore, J. Weekes, D. G. Hardie, Evidence that AMP triggers phosphorylation as well
561 as direct allosteric activation of rat liver AMP-activated protein kinase. A sensitive
562 mechanism to protect the cell against ATP depletion. *Eur J Biochem* **199**, 691-697
563 (1991).
564 45. B. B. Kahn, T. Alquier, D. Carling, D. G. Hardie, AMP-activated protein kinase: ancient
565 energy gauge provides clues to modern understanding of metabolism. *Cell Metab* **1**, 15-
566 25 (2005).
567 46. L. Dubrovsky *et al.*, Inhibition of HIV Replication by Apolipoprotein A-I Binding Protein
568 Targeting the Lipid Rafts. *mBio* **11** (2020).
569 47. L. Huang *et al.*, Inhibitory effects of p38 inhibitor against mitochondrial dysfunction in the
570 early brain injury after subarachnoid hemorrhage in mice. *Brain Res* **1517**, 133-140
571 (2013).
572 48. K. Young, H. Morrison, Quantifying Microglia Morphology from Photomicrographs of
573 Immunohistochemistry Prepared Tissue Using ImageJ. *J Vis Exp* 10.3791/57648 (2018).
574 49. Q. Xu *et al.*, Stress induced aging in mouse eye. *Aging Cell* **21**, e13737 (2022).

575

576

577

578 **Figures and Tables**

579

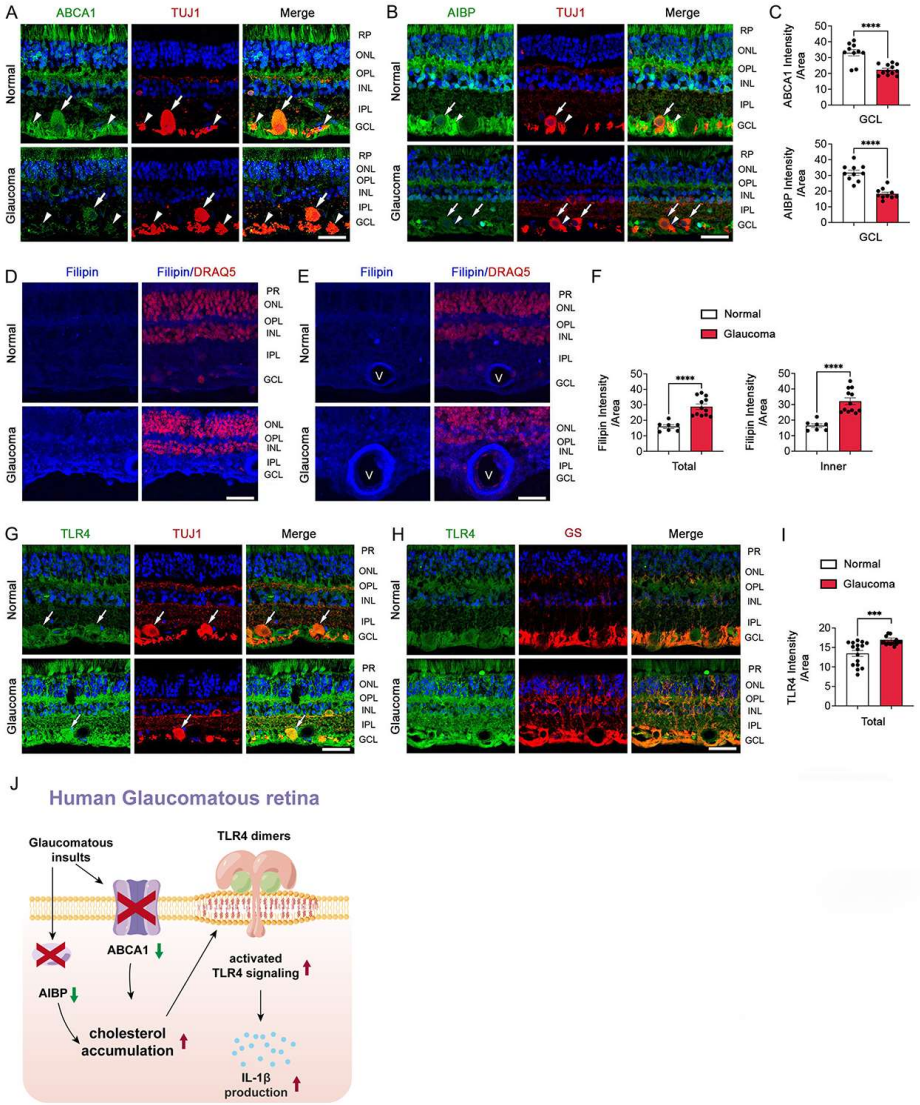

580

581 **Fig. 1. Glaucomatous human retina displays decreased AIBP and ABCA1 protein**
582 **expression and increased cholesterol content and TLR4 and IL-1β expression.** (**A**)
583 Representative retina images for ABCA1 (green) and TUJ1 (red) immunoreactivities. Arrows and
584 arrowheads indicate ABCA1 immunoreactivity co-labeled with TUJ1 in RGC somas and RGC
585 axon bundle, respectively. (**B**) Representative retina images for AIBP (green) and TUJ1 (red)
586 immunoreactivities. Arrows and arrowheads indicate AIBP immunoreactivity co-labeled with TUJ1
587 in RGC somas and RGC axon bundle, respectively. (**C**) Quantitative fluorescent intensity of
588 ABCA1 and AIBP immunoreactivities in the GCL of the glaucomatous retina. (**D**) Representative
589 retina images for filipin (blue) and DNA (DRAQ5, red) staining for total retinal layer. (**E**)
590 Representative retina images for filipin (blue) and DNA (DRAQ5, red) staining for retinal blood
591 vessels. (**F**) Quantitative fluorescent intensity of filipin staining in the total and inner layers of the
592 glaucomatous retina. (**G**) Representative retina images for TLR4 (green) and TUJ1 (red)
593 immunoreactivities. Arrows indicate TLR4 immunoreactivity co-labeled with TUJ1 in RGC somas.

594 (**H**) Representative retina images for TLR4 (green) and GS (red) immunoreactivities in Müller glia.
595 (**I**) Quantitative fluorescent intensity of TLR4 immunoreactivity in the total layer of the
596 glaucomatous retina. (**J**) Schematic for the effect of increased levels of cholesterol on TLR4/IL-1β
597 activation in the human glaucomatous retina. n = 10-16 sections from 2 eyes from control
598 subject, and n = 10-16 sections from 4 eyes from patients with glaucoma. Error bars represent
599 SEM. Statistical analysis was performed using Student's *t*-test. ***$P < 0.001$ and ****$P < 0.0001$.
600 Scale bars, 20 μm.

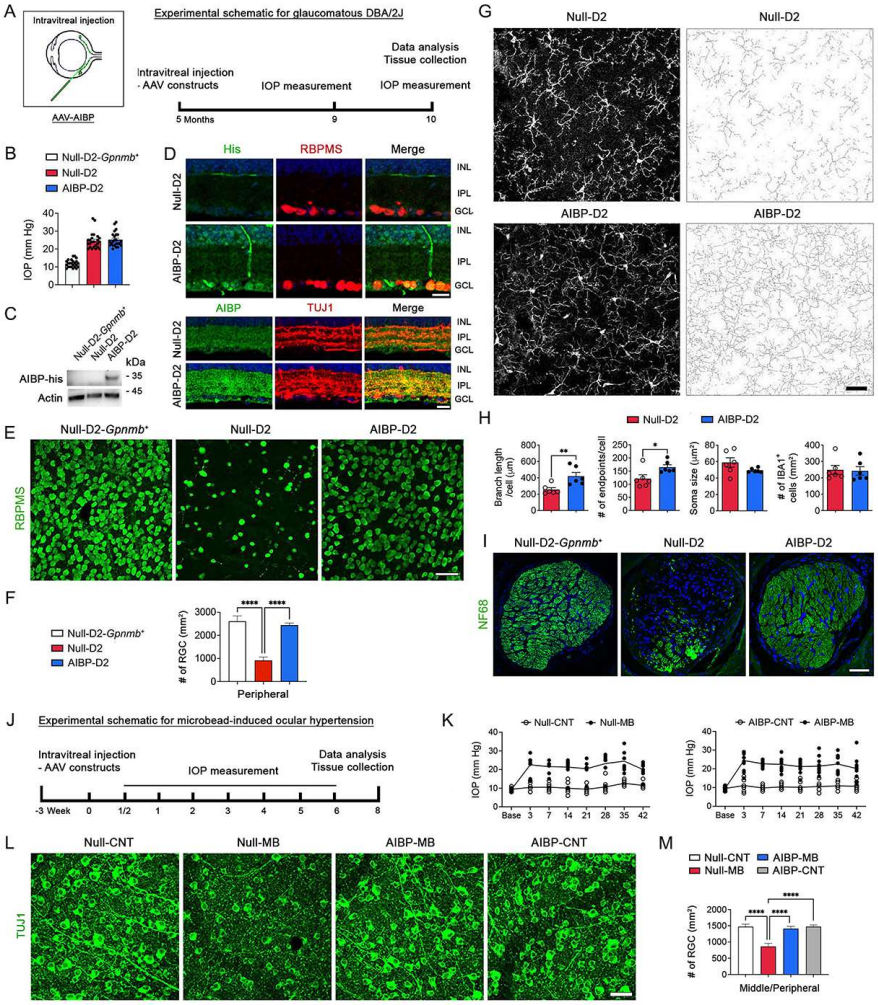

601

602 **Fig. 2. AIBP expression protects RGCs in mouse models of glaucoma.** (**A**) Experimental
603 schematic and timeline of AAV injection, IOP measurement, tissue collection and data analysis in
604 D2 mice. (**B**) IOP measurement in 10-month-old D2-*Gpnmb*⁺, Null-D2 and AIBP-D2 mice (*n* = 24
605 mice per group). (**C**) Representative image of western blot for AIBP expression, detected with an
606 anti-His antibody, in the retinas of Null-D2-*Gpnmb*⁺, Null-D2 and AIBP-D2 mice (*n* = 3 retinas
607 from 3 mice per group). (**D**) Representative retinal images for His (green) and RBPMS (red)
608 immunoreactivities or AIBP (green) and TUJ1 (red) immunoreactivities in Null-D2 and AIBP-D2
609 mice. (**E**) Representative retina wholemount images for RBPMS (green)-positive RGCs in the
610 peripheral retina. (**F**) Quantitative analysis of RGC numbers in the peripheral areas of the retina
611 (*n* = 5 retina wholemounts from 5 mice for age-matched control Null-D2-*Gpnmb*⁺ mice, *n* = 8
612 retina wholemounts from 8 mice for glaucomatous Null-D2 mice and *n* = 12 retina wholemounts
613 from 12 mice for glaucomatous AIBP-D2 mice). (**G**) Representative retinal wholemount images
614 for IBA1-positive microglial cells in the middle retina of Null-D2 and AIBP-D2 mice. (**H**)
615 Quantitative analysis of branch length (per cell), number of endpoints (per cell), soma size and
616 IBA1-positive number in microglial cells the middle retina (*n* = 6 retinal wholemounts from 6 mice
617 for Null-D2 and AIBP-D2 mice). (**I**) Representative ONH images for NF68 (green)-positive axons
618 in Null-D2-*Gpnmb*⁺, Null-D2, and AIBP-D2 mice. (**J**) Experimental schematic and timeline of AAV
619 transduction, IOP measurement, tissue collection and data analysis in a mouse model of
620 microbead-induced ocular hypertension. (**K**) Monitoring of IOP elevation in MB-injected C57BL/6J
621 mice (*n* = 9-11 mice per group). (**L**) Representative whole-mounted retina images for TUJ1

(green) immunoreactivity in the middle/peripheral area from MB-injected C57BL/6J mice. (**M**) Quantitative analysis of RGC number in the middle/peripheral areas of the retina (*n* = 5 retina wholemounts from 5 mice for age-matched Null-CNT and AIBP-CNT mice; *n* = 7 retina wholemounts from 7 mice for Null-MB mice; *n* = 9 retinal wholemounts from 9 mice for AIBP-MB mice). Error bars represent SEM. Statistical analysis was performed using one-way ANOVA and Tukey's multiple comparisons test. ***P* < 0.01 and *****P* < 0.0001. Scale bars, 20 μm (D) and 50 μm (E and G).

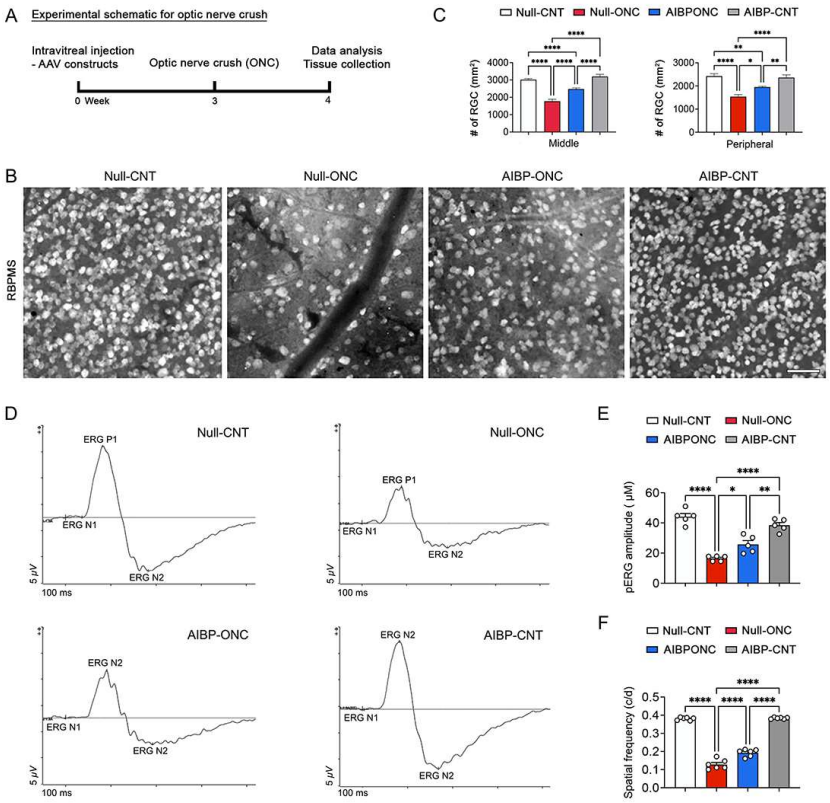

Fig. 3. AIBP expression protects RGCs in a mouse model of optic nerve crush. (**A**) Experimental schematic and timeline of AAV transduction, ONC, tissue collection and data analysis in the mouse model of ONC. (**B**) Representative whole-mounted retinal images for RBPMS (gray) immunoreactivities in the middle and peripheral area from ONC-induced C57BL/6J mice. (**C**) Quantitative analysis of RGC number in the middle/peripheral areas of the retina (*n* = 5 retina wholemounts from 5 mice per group). (**D**) Representative recording graphs of pERG amplitude. (**E**) pERG amplitudes analyses (*n* = 5 mice per group). (**F**) Spatial frequency by optomotor response analyses (*n* = 5 mice per group). Note that AIBP expression restores visual function in ONC mice. Error bars represent SEM. Statistical analysis was performed using one-way ANOVA and Tukey's multiple comparisons test. **P* < 0.05, ***P* < 0.01, ****P* < 0.001 and *****P* < 0.0001. Scale bar, 50 μm.

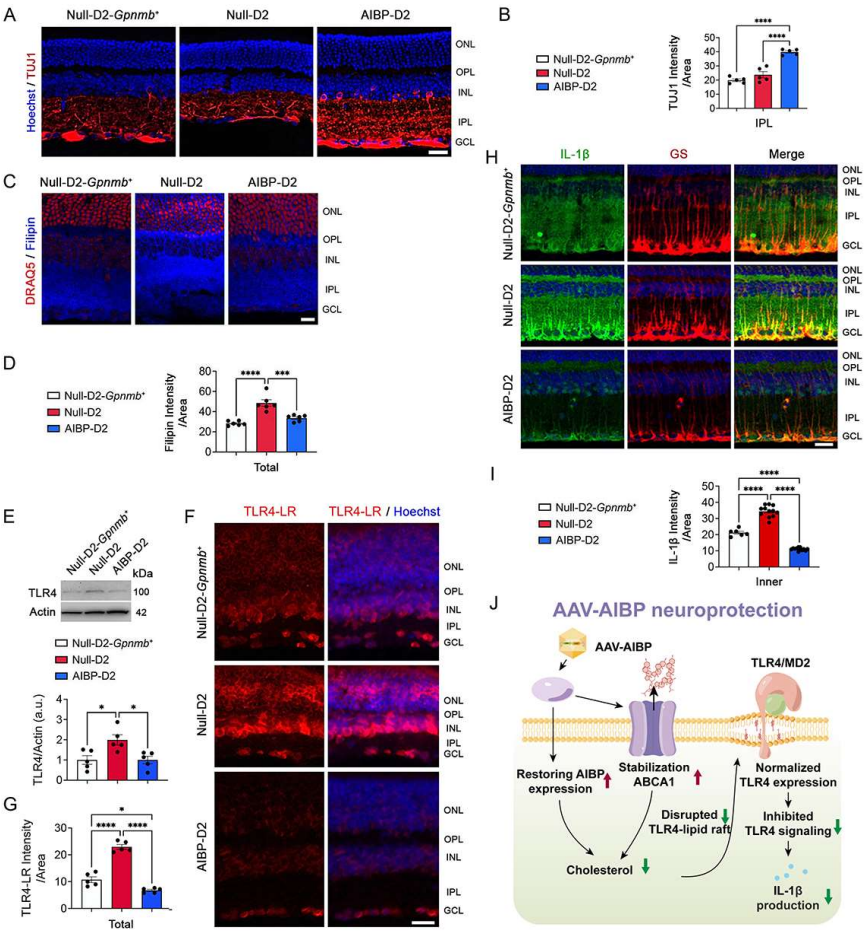

Fig. 4. AIBP expression decreases cholesterol deposition and TLR4 and IL-1β expression in glaucomatous D2 retina. (**A**) Representative retina images for TUJ1 immunoreactivity. (**B**) Quantitative fluorescent intensity of TUJ1 intensity in the IPL of the glaucomatous retina (*n* = 5 retina sections from 3 mice per group). (**C**) Representative retina images for filipin (blue) and DNA (DRAQ5, red) staining for total retinal layer. (**D**) Quantitative fluorescent intensity of filipin staining in the total and inner layers of the glaucomatous retina (*n* = 6 retina sections from 3 mice per group). (**E**) Western blot analysis for TLR4 protein expression in the retinas of 10-month-old D2 mice (*n* = 5 mice per group). (**F**) Representative retina images of PLA detection of TLR4-lipid raft (LR) proximity (red). (**G**) Quantitative fluorescent intensity of PLA detection of TLR4-LR proximity in the total layer of the glaucomatous retina (*n* = 5 retina sections from 3 mice per group). (**H**) Representative retina images for IL-1β (green) and GS (red) immunoreactivities in Müller glia. (**I**) Quantitative fluorescent intensity of IL-1β immunoreactivity in the total layer of the glaucomatous retina (*n* = 6 retina sections from 3 mice per group). (**J**). Schematic for RGC survival by AAV-AIBP-induced reduction of retinal cholesterol deposition and of TLR4-LR formation. Error bars represent SEM. Statistical analysis was performed using one-way ANOVA and Tukey's multiple comparisons test. *$P < 0.05$, ***$P < 0.001$ and ****$P < 0.0001$. Scale bars, 20 μm.

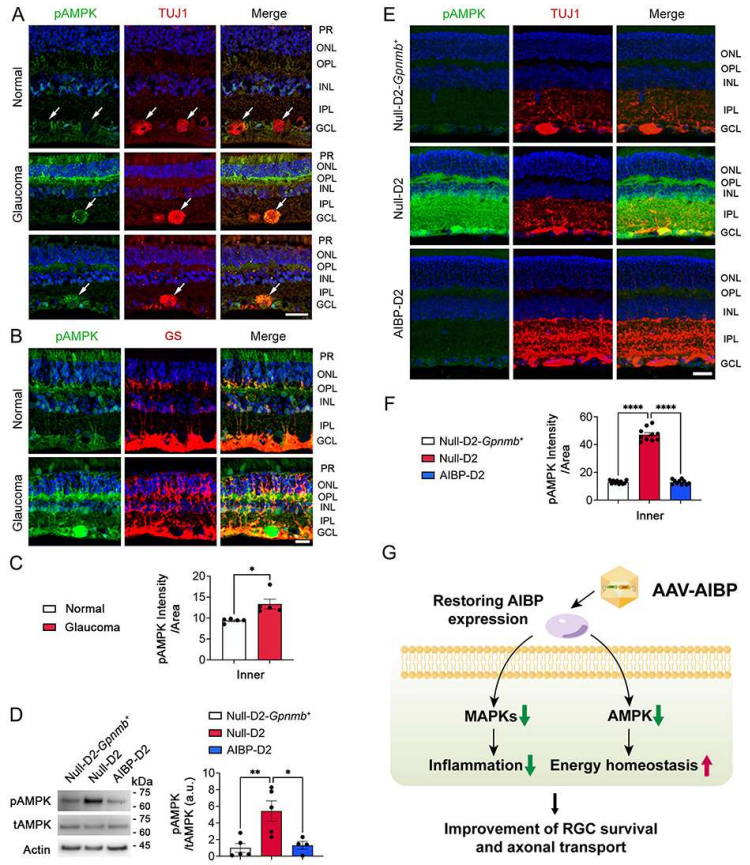

Fig. 5. AIBP expression inhibits AMPK hyperactivation in the glaucomatous retina. (**A**) Representative retina images for phospho-AMPK (pAMPK, green) and TUJ1 (red) immunoreactivities in the glaucomatous human retina. (**B**) Representative retina images for pAMPK (green) and GS (red) immunoreactivities in Müller glia of the glaucomatous human retina. (**C**) Quantitative fluorescent intensity of pAMPK immunoreactivity in the inner layer of the glaucomatous human retina (n = 5 retina sections from 2 eyes from control subject and n = 5 retina sections from 4 eyes from patients with glaucoma). (**D**) Western blot analysis of pAMPK in glaucomatous D2 retina (n = 4-5 retinas from 4-5 mice per group). (**E**) Representative retina images for pAMPK (green) and TUJ1 (red) immunoreactivities in glaucomatous D2 retina. (**F**) Quantitative fluorescent intensity of pAMPK immunoreactivity in the inner retina of glaucomatous D2 mice (n = 10 retina sections from 3 mice per group). (**G**) Schematic for reduction of retinal MAPKs and AMPK activations by AAV-AIBP. Error bars represent SEM. Statistical analysis was performed using Student's t-test or one-way ANOVA and Tukey's multiple comparisons test. *P < 0.05, **P < 0.01, and ****P < 0.0001. Scale bars, 20 μm.